Materials Studies
Preliminary Status Report
Transmutation Science Group

Neutron Leakage from a Lead-Bismuth Target (Diameter = 20 cm, Length = 50 cm)

Neutron Leakage from a Lead-Bismuth Target
(Diameter = 20 cm, Length = 50 cm)

Document Number:
LA-UR-02-5552
AAA-02-204
Revision 0
August 2002

Abstract:
Initial experiments were conducted at the Target 2 facility (commonly called the Blue Room) of the Los Alamos Neutron Science Center (LANSCE) to support the Advanced Accelerator Applications (AAA) Program. The experiments consisted of irradiating a solid lead-bismuth target (diameter=20 cm, length=50 cm) with the 800-MeV proton beam and measuring the neutron emission from the target by two different methods—activation foils and time-of-flight (TOF) measurements.

For the activation foil measurements, numerous foil packets were assembled and mounted on the target for a specified period. One foil packet was irradiated during the initial period on Dec. 1, 2001. The foils were then removed and counted to obtain preliminary estimates of activation levels and to identify peaks of interest for specific reactions. Preliminary results are reported here. Ten foil packets were then mounted on the target and a second irradiation was conducted on Dec. 2, 2001. The foils were then removed and the gamma activity counted at the LANSCE facility and at the analytical laboratory at TA-48.

Upon completion of the foil activation runs, TOF measurements were performed using two flight paths (7.5° and 30°) on Dec. 2-4, 2001. The spectra were measured for three different locations of the target—the focal point of the beam tubes at the front face of the target, 20 cm into the target, and 40 cm into the target. Initial results are included in this report.

The irradiations and TOF measurements were conducted without incident and with minimal personnel exposure. Preliminary results indicate that both techniques for measuring the neutron leakage provide useful and complementary information. The activation foils provide significant quantities of integral reaction data that can be used for spectral unfolding, with errors representative of the uncertainties in the nuclear data. The TOF measurements provide very detailed information regarding the neutron spectra in a small solid angle (i.e., double differential data).

Author:

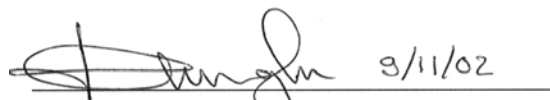AAA-Materials Studies
Los Alamos National Laboratory

Michael R. James/Date   9-9-02

Approval:

Project Leader, Transmutation Science
AAA-Los Alamos National Laboratory

Kemal O. Pasamehmetoglu/Date   9/11/02

Additional Authors

R.T. Klann
G.L. Morgan
K.A. Wolshun
E.J. Pitcher
M.A. Paciotti
J.M. Oostens
V. Tcharnotskaia

Distribution List

AAA Project File	H816
RMDC (BREI)	C341
M.W. Cappiello	H816
M.R. James	K575
R.T. Klann	ANL
N. Li	H816
S.A. Maloy	H809
G.L. Morgan	H803
J.M. Oostens	Columbia, KY
K.O. Pasamehmetoglu	H816
M.A. Paciotti	H846
E.J. Pitcher	H805
V. Tcharnotskaia	H855
K.A. Wolshun	H855

Table of Contents

List of Figures

List of Tables

List of Acronyms

AAA	Advanced Accelerator Applications
ADC	Analog-to-digital converter
ADTF	Accelerator-Driven Test Facility
FWHM	Full width half maximum
HPGe	High-Purity Germanium (detectors)
ICT	Integrating current transformer
LANL	Los Alamos National Laboratory
LANSCE	Los Alamos Neutron Science Center
LBE	Lead-bismuth eutectic
MCNPX	Computer code used in modeling high-energy physics reactions
NIST	National Institute of Standards and Technology
PCGAP	Gamma-ray analysis program
TOF	Time-of-flight
WNR	Weapons Neutron Research

1. Introduction

Spallation neutron sources create high-energy neutrons whose energies extend up to the incident proton energy. In the design of accelerator-driven waste transmuters, the high-energy neutrons that leak from the spallation target have three practical implications. First, they dominate the shield design because they have long attenuation lengths (18 cm in steel). Second, they lead to the production of source neutrons in the fuel region, which generates a spatially dependent neutron source that influences the power density distribution in the blanket. Third, they dominate the production of H and He atoms in the steel structural elements that reside in the multiplier region near the target. This gas production limits the lifetime of structural materials near the target.

As a means of reducing gas production in structural materials in the multiplier region, a buffer region consisting of high-atomic-mass material may be placed between the target and multiplier. This buffer attenuates high-energy neutrons that leak from the target into the multiplier. Additionally, the configuration of the buffer and the associated beam rastering parameters are variables available to the accelerator-driven waste transmuter designer (specifically the Accelerator-Driven Test Facility or ADTF designer) for adjusting the multiplier power distribution.

MCNPX is the physics code being used heavily in the design process to predict the creation and transport of high-energy particles in accelerator-driven waste transmuter conceptual design studies. Data are necessary to validate that MCNPX is correctly predicting the production and transport of neutrons from the spallation target. This series of experiments will provide benchmark data regarding the magnitude, energy spectrum, and spatial profile of neutrons leaking from the radial surface of a cylindrical spallation target. Lead-bismuth eutectic (LBE) is a prime candidate for target material in current accelerator-driven waste transmuter conceptual designs. Therefore, this series of irradiation experiments focuses on spallation targets made of LBE. Other spallation target candidate materials could be studied in the future if the AAA Project determines it is a priority.

To evaluate the effectiveness of a buffer in modifying the energy spectrum of neutrons leaking from the spallation target into the buffer or blanket regions, measurements will be performed for several different LBE target radii with a fixed target length exceeding the maximum range of the 800-Mev protons in LBE. Three target diameters will be used during the measurement campaign: 5 cm, 10 cm, and 20 cm. The target length is 50 cm. These values were selected to be prototypical of current designs for the ADTF. In addition, the beam entry radius will be varied for one or more of these targets, creating additional data sets for comparison with MCNPX calculations.

Time-of-flight (TOF) measurements and activation foils are used to perform the neutron measurements. The activation foils are assembled into foil packets and are described in the experiment description below. Four neutron flight paths will be used for the TOF measurements.

This report describes the preliminary results for the initial target irradiations conducted Dec. 1-4, 2001. The initial target irradiations were conducted using a solid LBE target with a diameter of 20 cm and a length of 50 cm.

For the activation foil measurements, numerous foil packets were assembled and mounted on the target for a specified period. One foil packet was irradiated during the initial period on Dec. 1, 2001. The foils from that packet were then removed and counted to obtain preliminary estimates of activation levels and to identify peaks of interest for specific reactions. Preliminary results are reported here. The 10 foil packets were mounted on the target and a second irradiation was conducted on Dec. 2, 2001. The foils were then removed and the gamma activity counted at the Los Alamos Neutron Science Center (LANSCE) facility and at the analytical laboratory at TA-48.

Upon completion of the foil activation runs, TOF measurements were performed using two flight paths (7.5° and 30°) during Dec. 2-4, 2001. The spectra were measured for three different locations of the target—the focal point of the beam tubes at the front face of the target, 20 cm into the target, and 40 cm into the target. Initial results are included in this report.

The goals of the initial target irradiation experiment were to:

1. provide initial experimental data for planning future irradiation campaigns,

2. provide experimental data of benchmark quality to be used for validation of MCNPX,

3. provide experimenters with practical experience for conducting these types of measurements and data analysis activities, and

4. further develop methods and improve techniques for spectral unfolding using integral reaction data from activation foils.

These initial target irradiations will be followed by fully instrumented LBE targets during future irradiation periods. The target and beam parameters will be varied for thorough studies of thick-target neutron leakage. The next target irradiation will include using all four available flight paths (7.5°, 30°, 60°, and 150°) and a full complement of activation foils along the entire length of the target. In addition, other flight paths will be considered for the measurement program.

Additional system parameters can be studied as part of continuing experiments. There is interest in studying different buffer materials, target materials, coolant materials, and coupled target-buffer geometries. In addition, follow-on measurements will be planned based on analysis of the data from the initial measurement series.

2. Experiment Description

The experiment was carried out in the Target 2 area at the Weapons Neutron Research (WNR) facility at LANSCE. Target 2 is a shielded room approximately 12 meters in diameter with a series of flight paths radiating from the center of the room, as shown in Figure 1. Proton beams up to 100 nA can be accommodated. Neutrons leaking from the target could be observed through two flight paths at angles of 7.5° and 30° with respect to the incident proton beam.
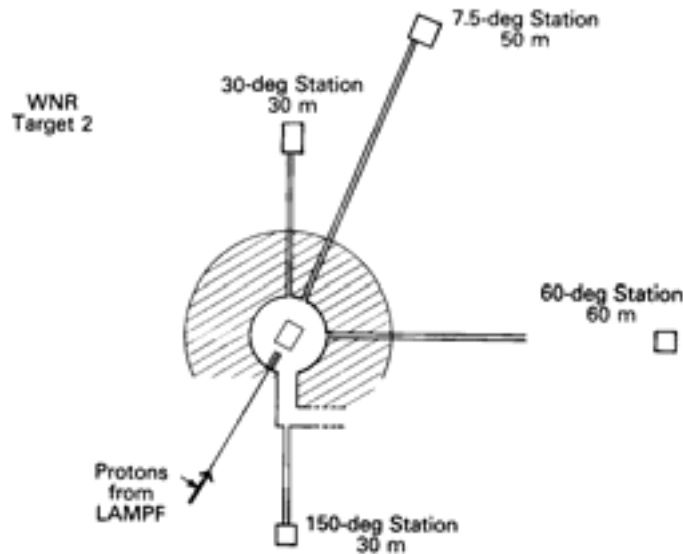
**Figure 1. Schematic diagram of WNR Target 2 and
the flight path used for neutron measurements.**

A schematic diagram of the experimental configuration is shown in Figure 2. The experimental equipment is described by subsystem based on the function of the components—the target and support equipment, TOF beamlines, activation foils and packets, gamma spectroscopy systems, and configuration of a foil packet irradiation performed in Target 4.

The proton beam was provided by the LANSCE accelerator. The proton beam exited the beamline vacuum through a thin stainless steel window, traveled about 2 meters through air, and then was incident on the target. A primary requirement for the measurement of proton interactions is the determination of the parameters of the incident beam. These parameters include the total integrated beam striking the target assembly in each irradiation, the position of the beam on the target, and the beam intensity profile. The beam monitor system is shown schematically in Figure 2.
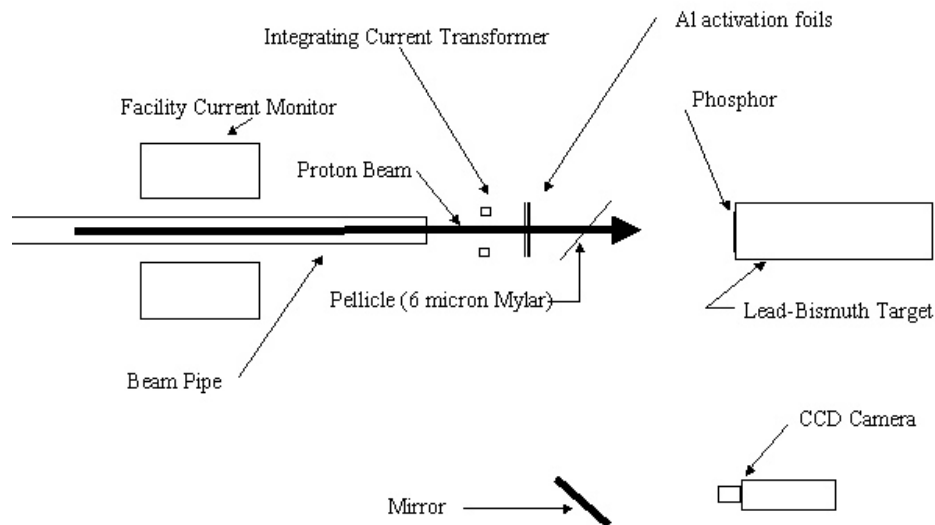
Figure 2. Schematic diagram of the experimental configuration showing the beam monitoring equipment.

2.1 Target and Support Equipment

The required dimensions for a cylindrical target for the neutron leakage experiment were 10-cm radius and 50-cm length. The target was made of solid LBE.

Lead-bismuth eutectic is an alloy with 44.5% lead and 55.5% bismuth. For this target the metal was purchased from Ney Smelting and Refining Co., Brooklyn, NY. The lead-bismuth purity as requested was 99.99%. An analysis of the lead-bismuth was performed after casting. The data sheet is shown in Appendix A.

The target was made by casting lead-bismuth in a cylindrical mold. An 8-inch-diameter steel pipe was machined to ensure a constant inside diameter and a smooth finish. A flat plate was welded to the end of the pipe to serve as the mold bottom.

Tape heaters were used to heat the mold, and ingots of lead-bismuth were melted inside until the level of the liquid metal reached height above 50 cm. The mold was chilled slowly from the bottom up by shutting off heaters and removing insulation from the bottom up. Cooling the mold in this fashion provided for the smallest chance of voids forming inside the final solid.

After the mold and the target were completely cooled, a machinist cut the mold wall axially in two places to remove it. The mold readily came off the target. The ends of the cylinder were then machined off to ensure that the flat ends of the target are

perpendicular to its sides and to achieve the proper length. Final target dimensions were 20.32 cm diameter and 50 cm length. It weighed about 171.4 kg or 377.85 lbs.

The target was weighed and its measured weight coincided with its calculated weight, demonstrating a lack of significant interior voids. The side surface near the top of the mold exhibited very small holes that were considered negligible.

The cylindrical lead-bismuth target had to be aligned axially with the proton beam. For that purpose a support was built. The target was placed horizontally on a 6-inch aluminum C-channel so that its side rested on the short sides of the channel and the channel wall faced down. Four 30-cm-long aluminum legs were welded to the corners of the C-channel's wider side to hold the target away from the main support table during the experiment. A 0.5-inch-thick aluminum plate was welded at the bottom for mounting and rigidity. A drawing of the target and support is shown in Figure 3. A photograph of the target and support is shown in Figure 4.
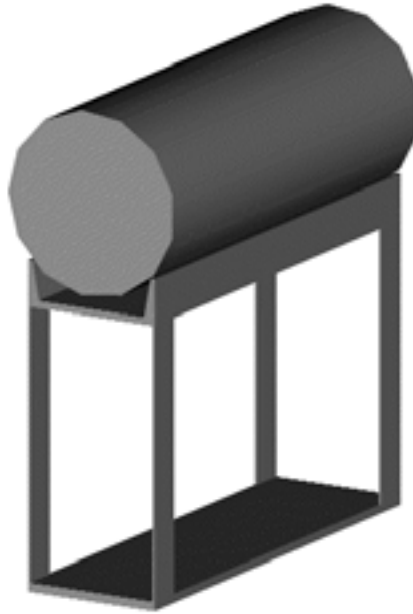
Figure 3. Schematic of LBE target on the aluminum support structure.

A remotely actuated positioning table was used to move the target axially during the experiment. The table was manufactured by H2W Technologies, Valencia, CA. It was sized to carry a 1500-lb load over 20 inches (50.8 cm) at a speed of less than 0.1 inch/sec with a minimum resolution of 0.01 inch (0.254 mm). The positioning table was essentially a sliding plate actuated by a servomotor and mounted on a 37.5-inch-long, 6.7-inch-wide support housing. The bottom plate of the target support was bolted to the positioning table sliding plate.

Figure 4. LBE target on the aluminum support structure.

The table motor was controlled by a programmable remote controller. The motor moved the sliding plate along the length of the support base. The whole assembly was bolted to a heavy-duty lift table that allowed for vertical position adjustment inside the Blue Room.

2.2 Time-of-Flight Beamlines

The beamlines for the TOF measurements were produced by existing equipment installed in the Blue Room. Figure 1 gives a schematic of Target 2, with the associated neutron flight paths. The 7.5° and 30° flight paths were used for these measurements. Calibrated plastic scintillators [1–8] were used to measure neutron TOF spectra for the higher neutron energies. ^{6}Li loaded glass scintillation counters [8] were also used in separate data collection runs and produced data on low-energy neutron leakage. The flight-path collimation used to define the field-of-view at the target position for these detectors is summarized in Table 1. A thorough description of the beamlines and collimation is provided in References 1–7.

Table 1. Flight Path Collimation and Field-of-View at the Target Location

	7.5° Flight Path	30° Flight Path
Field of View Collimator Diameter (inches)	4.00	4.00
Distance from Origin (inches)	168	155
Distance to Detector (inches)	2013.6	1175.1
Field of View at Origin (inches)	4.36	4.61
Second Collimator Diameter (inches)	3.52	3.75
Distance from Origin (inches)	482	234
Field of View at Origin (inches)	4.63	4.68
Minimum Field of View (inches)	4.36	4.61

2.3 Activation Foils and Foil Packets

To gather information about the energy spectrum of the neutrons emitted from the LBE target, activation foils were selected with the following characteristics:

1. The element should lead to several (n,*x*n) reactions, each one with increasing threshold with increasing *x*.

2. Accepted dosimetry cross-section data must exist for the reactions of interest.

3. The element should have a high Z to be insensitive to proton-induced reactions.

4. The element should have a single isotope to avoid ambiguities in the identification of the reaction producing the secondary products.

5. The reaction products must have half-lives larger than about one hour to allow collecting the foils and bringing them to the counting area.

6. The reaction products must have several strong gamma lines for easy recognition.

7. If possible, the half-life should be long enough to be measured quantitatively with the limited number of detectors available.

The foil packets consisted of several foil materials packaged together for simultaneous irradiation. The materials used for most foil packets were Bi, Nb, In, Co, Ni, Cu, Fe, Al, Au, Cd-covered Au, Rh, Ti, Zn, Lu, and Tb. The materials were chosen based on the above criteria, as well as to provide working experience with a few experimental foils such as Lu, Bi, and Tb.

The foils were cut from rolled sheet material and were generally 1 cm square and 0.1 or 0.25 mm thick. The bismuth material was cut from a solid rod (1 cm diameter) and sanded to remove rough edges. Each foil was weighed and scribed with an identification

mark before being placed into a packet, as shown in Figure 5. The foils were weighed on a Mettler H80 balance that was calibrated before use. Fourteen foil packets were made to handle the various irradiations. Due to a shortage of foil material, not all foil packets were complete; only the stacks labeled 1 through 4 contained the Rh and Tb materials.
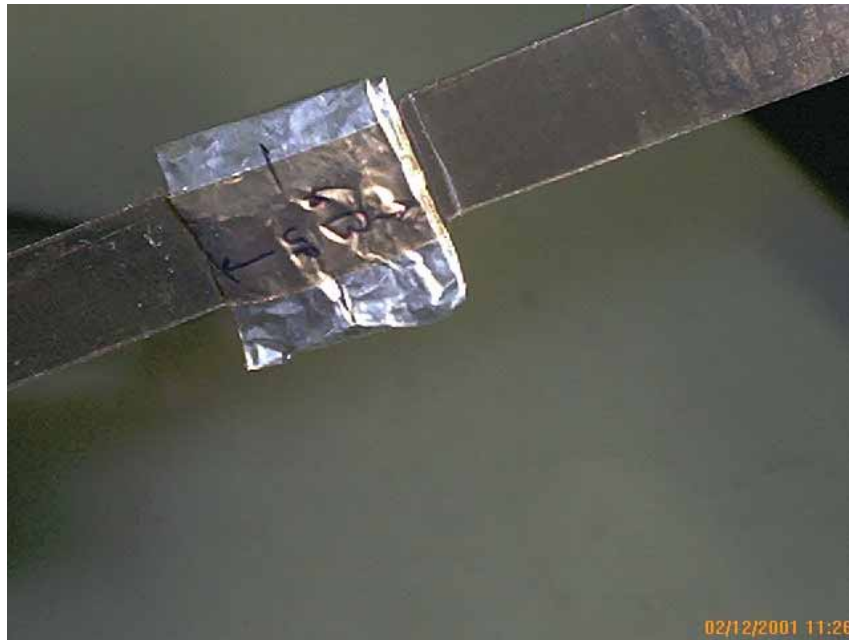
**Figure 5. Assembled foil packet wrapped in Al foil
before mounting on the target with mylar tape.**

2.4 Gamma Counting Systems

The majority of the gamma-ray counting was performed by the established counting laboratory in the LANL Isotope and Nuclear Chemistry department (at TA-48). The laboratory at TA-48 contains germanium detectors that are permanently stationed and routinely calibrated. Samples are mounted on cards that are automatically fed to the detectors. The automated systems count, analyze, and report the results to the experimenter. Because TA-48 is not located in close proximity to the Blue Room, the foils must be transported to the counting laboratory. As a result of the transit time, nuclides with very short half-lives cannot be counted effectively at TA-48.

To obtain gamma ray spectra at the earliest available times after irradiation, a local counting station with two germanium spectrometers was configured in the staging area at the LANSCE facility. One of the detectors (Detector 3) is horizontally mounted. The samples are mounted on aluminum cards that are prepositioned to center the sample on the detector. By using an inside caliper, sample-to-detector distance can be set and measured with an accuracy of 0.2 mm. Samples were placed at accurately measured distances of 0.0 cm, 5.0 cm, or 10.0 cm, as shown in Figure 6. The other detector (Detector 7) was located within a lead-shielded cave (Figure 7). The cave assembly

contains a mounting fixture (Figure 8), which allows easy mounting of samples at fixed reproducible distances. The characteristics of the detectors are given in Table 2.

**Figure 6. Horizontally mounted HPGe (Detector 3)
counting a sample that is mounted on an aluminum card.**

Figure 7. HPGe 7 inside of low-background lead shielded cave.
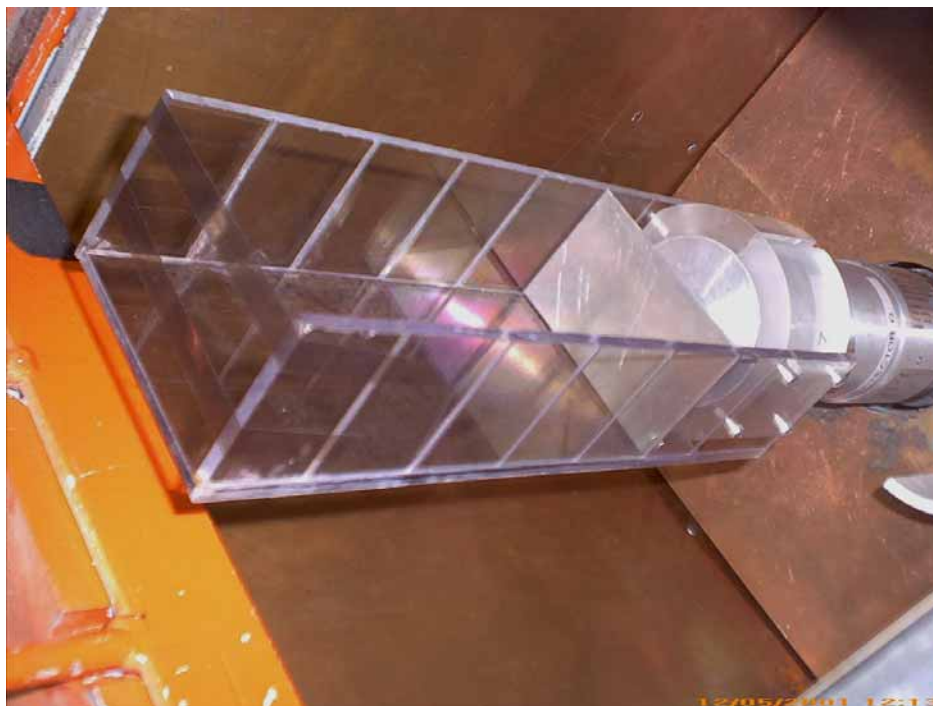
**Figure 8. The internals of the shielded cave of
Detector 7 showing the sample mounting assembly.**

Table 2. Characteristics of HPGe Detectors 3 and 7

Detector Number	Model Number	Crystal Diameter	Crystal Length	Window	FWHM @ 1.33 MeV
3	GEM-40190-P	64.3 mm	59.9 mm	1.0 mm Al	1.79
7	GEM-40190-P	66.5 mm	64.0 mm	1.0 mm Al	1.79

The gamma spectra were collected using an Ortec DSPEC multi-channel channel analyzer system connected to a personal computer running *Gamma Vision*. The spectra were analyzed with a gamma-ray analysis program called *PCGAP*. This program can automatically fit a Gaussian function to spectral peaks or perform an interactive fit by the operator specifying the peak-fitting limits and background. The analysis program locates the photopeaks by zero area correlation methods where the sensitivity has been optimized. The peak areas are determined by Gaussian function least-squares fitting and step function background subtraction. The photopeak energy location is determined by the peak analysis and energy calibration functions. The possible radionuclide identifications are then determined by comparing the observed photopeak energies with the known photon energies of the radionuclides residing in the decay data library. The radionuclide activities are then calculated based on the detector efficiency for the source-to-detector distance used. Where multiple photopeaks are associated with a radionuclide, the activity of each peak is determined and a weighted average of all peaks is computed based on the radionuclide emission probabilities and uncertainty in the peak areas.

Dead time was limited to <5% for the highest activity samples by adjusting the sample to detector distance. Sample-to-detector distance was 10 cm or less for all cases.

Measurements of gamma-ray standards were used to establish the full-energy gamma-ray peak counting efficiencies for each detector and counting distance used in the experiment. These standard sources provide numerous gamma energies that cover the energy range from 88 to 1836 keV. The energy dependence of the efficiency for each detector was established by spectra obtained at an earlier date (October 2000) with the mixed standard (QCD 2000) with characteristics given in Table 3.

Table 3. Source Characteristics for Source QCD2000 (Amersham Source Number 2773QB)

Nuclide	Energy (keV)	Emission Rate on 8/1/00 (Gammas/sec)	Standard Deviation (%)	Half-life (days)
Cd-109	88.03	645	3.1	461.4
Co-57	122.1	579	0.8	271.79
Ce-139	165.9	683	0.8	137.64
Hg-203	279.2	1967	0.8	46.612
Sn-113	391.7	2074	2.1	115.09
Sr-85	514	3877	1.3	64.84
Cs-137	661.7	2480	1.1	10983.0
Y-88	898	6174	0.9	106.65
Co-60	1173	3352	0.8	1925.2
Co-60	1333	3355	0.8	1925.2
Y-88	1836	6526	0.8	106.65

Using the automated efficiency function generator in *PCGAP*, efficiency files were made for each detector at 5 cm and 10 cm source-to-detector distances. Figure 9 is an example of a fifth-order fit in the Log of efficiency vs. Log of energy.
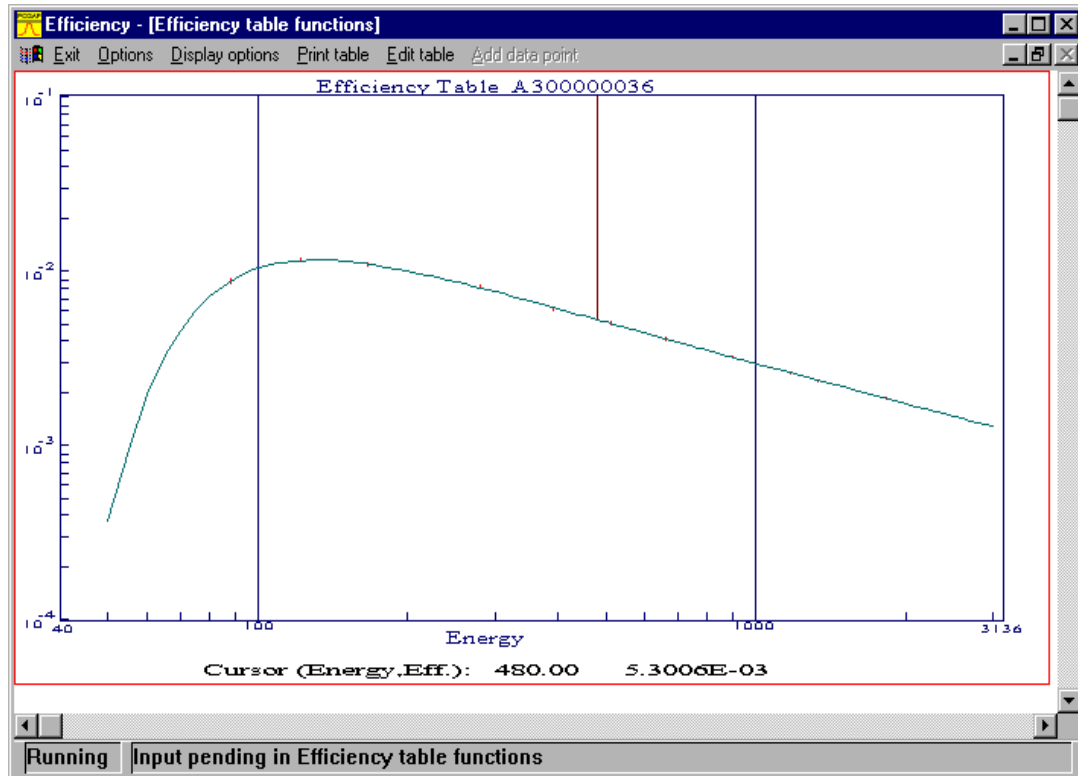
**Figure 9. Fitted efficiency function (function 36) for Detector 3.
Data points are seen in red at the energies of Table 3.**

Since the absolute calibration of the detectors must be done concurrently with the foil counting, another calibration standard (Amersham Radiological Source QCD1 number 2582QB manufactured in 1998) was employed. Its characteristics are listed in Table 4.

Spectra obtained with this source (QCD 1998) are summarized in Table 5, which also serves as a test of the four efficiency Functions 35, 36, 37, and 38. The table lists the deviations of activities (calculated with the four efficiency Functions) from those expected from Table 4. These deviations test the accuracy of the efficiency fitting functions, the source-to-detector positioning accuracies, and the stability of the detectors over 14 months. Significant deviations are seen for Detector 3.

Table 4. Source Characteristics for Source QCD1998 (Amersham Source Number 2582QB)

Nuclide	Energy (keV)	Emission Rate on 2/1/98 (Gammas/sec)	Standard Deviation (%)	Half-life (days)
Cd-109	88.03	621	2.6	461.4
Co-57	122.1	569	2.2	271.79
Ce-139	165.9	680	4.9	137.64
Hg-203	279.2	1918	2.5	46.612
Sn-113	391.7	2046	5.3	115.09
Sr-85	514	3777	2.4	64.84
Cs-137	661.7	2341	2.5	10983.0
Y-88	898	6059	3.2	106.65
Co-60	1173	3807	0.9	1925.2
Co-60	1333	3811	0.8	1925.2
Y-88	1836	6404	3.2	106.65

Table 5. Deviations of Measured Activities of the Amersham Calibration Standard QCD 1998 from the Expected Values

	Nuclide				
	Cd-109	Co-57	Cs-137	Co-60	Co-60
Energy (keV)	88.03	122.1	661.7	1173	1333
Detector 3 deviation of A32C0501000 QCD98 at 5 cm with Efficiency 35 (%)	12.59	-2.12	6.80	5.66	7.06
Error in fitting of peaks of QCD98 (%)	3.73	7.68	1.05	0.74	1.11
Detector 3 deviation of A32C0401000 QCD98 at 10 cm with Efficiency 36 (%)	8.60	—	2.77	3.94	2.97
Error in fitting of peaks of QCD98 (%)	11.15	—	0.72	1.01	1.22
Detector 7 deviation of A72C0101000 QCD98 at 5 cm with Efficiency 37 (%)	0.04	8.24	3.99	-0.17	0.90
Error in fitting of peaks of QCD98 (%)	1.55	4.17	2.26	1.63	1.31
Detector 7 deviation of A73C0201000 QCD98 at 10 cm with Efficiency 38 (%)	3.94	2.65	2.40	-1.13	1.45
Error in fitting of peaks of QCD98 (%)	3.79	13.80	2.28	0.95	2.19
Detector 7 deviation of A74C1201000 QCD98 at 10 cm with Efficiency 38 (%)	0.36	3.90	1.94	-0.94	2.33
Error in fitting of peaks of QCD98 (%)	3.87	5.33	2.34	1.65	1.54

As the actual distances between the detector face and the calibration sources differ slightly from the nominal values presented in Table 5, corrections were made assuming a simple model of the detector. The effective center of the detector is found by comparing the efficiency of the detector at two or more distances and finding the distance to the effective center so that a $1/r^2$ dependence is obtained where r is the distance between the point source and the effective center of the detector. The energy dependence of the distances to the effective center is given in Table 6.

Activities are obtained by the equation, $A = \dfrac{\gamma/s}{BR\varepsilon}$, where the efficiency is $\varepsilon = \dfrac{a}{(d + d_{ec})^2}$,

a is a constant, d is the source-to-detector distance, and d_{ec} is the distance to the effective center in Table 7.

Table 6. Computed Distances for Detector-to-Sample Spacing

Energy (keV)	Distance from the Detector Face to the Effective Center of Detector 3 (cm)	Distance from the Detector Face to the Effective Center of Detector 7 (cm)
88	2.33	2.09
122.1	2.66	2.32
165.9	2.43	2.40
279.2	2.97	2.77
391.7	2.97	2.90
514	3.08	3.10
661.7	3.21	3.21
898	3.47	3.16
1173	3.65	3.60
1333	3.47	3.46
1836	3.78	3.51

Table 7. Deviations of Measured Activities of the Amersham Calibration Standard QCD 1998 from the Expected Values*

	Nuclide				
	Cd-109	**Co-57**	**Cs-137**	**Co-60**	**Co-60**
Energy (keV)	88.03	122.1	661.7	1173	1333
Detector 3 deviation of A32C0501000 QCD98 at 5 cm with Efficiency 35 at 5.25 cm (%)	5.28	-8.22	0.58	-0.20	1.01
Detector 3 deviation of A32C0401000 QCD98 at 10 cm with Efficiency 36 at 10.2 cm (%)	5.16	—	-0.28	0.96	-0.02
Detector 7 deviation of A72C0101000 QCD98 at 5.1 cm with Efficiency 37 at 5.15 cm (%)	-1.34	6.80	2.75	-1.31	-0.27
Detector 7 deviation of A73C0201000 QCD98 at 10.1 cm with Efficiency 38 at 10.15 cm (%)	3.09	1.83	1.63	-1.85	0.71
Detector 7 deviation of A74C1201000 QCD98 at 10.09 cm with Efficiency 38 at 10.15 cm (%)	-0.62	2.90	1.02	-1.80	1.43

* where the distances of the calibration standard QCD 2000 have been adjusted to normalize the QCD 2000 efficiency functions to the absolute efficiency measurement (QCD 1998) taken concurrently with the foil activation data. The Detector 3 deviations are now nearly within the uncertainties given in Table 4.

The efficiency measurements were done with the QCD 2000 source in Table 3 at

distances denoted as d_{cal} in the equation, $\varepsilon_{cal} = \dfrac{a}{(d_{cal} + d_{ec})^2}$, where the constant is the

same as the previous expression for each detector. Adjustments in the reported activities are then made from the equation

$$\varepsilon_{cal} = \frac{\gamma / s}{BR\varepsilon} \frac{(d + d_{ec})^2}{(d_{cal} + d_{ec})^2} \tag{1}$$

The deviations for Detector 3 in Table 5 are suggestive that the d_{cal} distances from the QCD 2000 source to the detector may have been slightly in error. The first suggestion is that there is a systematic shift in the reported activities, and secondly that the shift is greater for lower energies, both of which can be approximately accounted for in Equation 1. Table 7 performs the normalization with Equation 1, where the adjusted distances d_{cal} for the QCD 2000 calibration source and the measured distances for the QCD 1998 verification source, d, are given in the headers. It was not thought that the d_{cal} distances could have been as far off as 2 or 2.5 mm, but they were not measured directly, only the position of the edge of the card was measured with respect to the edge of the detector. Equation 1 and Table 7 give an adequate normalization of the efficiency functions to QCD 1998 and form the basis for the calibration of the experiment.

2.5 Target 4 Configuration

As part of the experiment, an irradiation of foils was conducted downstream of Target 4. The purpose of this irradiation was to provide a well-characterized neutron spectra in which a foil packet was irradiated. The results of spectral unfolding from the activation foil data could then be directly compared to results from the TOF measurement. Two foil stacks were used, 1 and 14. They were placed on top of each other and then mounted on an Al plate. The Al plate was then placed in a location in the 30L beamline of Target 4, just past a fission detector as shown in Figures 10 and 11.

Figure 10. Picture of Al plate with foil packets 1 and 14 mounted on front face.

Figure 11. Picture of the plate and foils mounted in the beamline.
The laser cross-hairs are just visible on the surface of the Al plate.

3. Experiment Plan and Conduct

The experiment was performed in accordance with the experiment task plan and was conducted without incident at the LANSCE Target 2 (Blue Room) and Target 4 facilities. A description of each irradiation is described below.

3.1 Target 2 Irradiations

The details regarding the irradiations in the Target 2 area are best described in timeline format as recorded in the logbooks. The irradiation was begun on Dec. 1 and irradiation activities continued through Dec. 4, when the LBE target was removed from the beamline. Results of the foil activations and TOF measurements are included in Section 4. A detailed description of proton-beam monitoring activities is also included.

December 1, 2001

07:00-07:30	Received approvals to operate, RWP review, and other administrative matters
07:30-08:00	Conducted pre-job briefing
08:00-11:00	Assembled target in beamline
11:20-12:00	Checked beam alignment
12:12-12:33	Mounted foil packet on target
12:43-15:34	Irradiation of target (first irradiation with activation foils)
16:00-16:30	Removed foils and transported to staging area
16:45-22:30	Counted foils in the staging area and set up overnight counting runs
19:30-20:30	Finished preparing foil packets

December 2, 2001

09:00-12:00	Mounted foil packets and checked beam alignment
12:11-16:12	Full Irradiation (second irradiation with full set of activation foils)
16:30-17:30	Removed foils, closed up for TOF
17:45-19:45	Set up, debug TOF measurement system, began foil counting
19:54-21:17	High-energy TOF measurement at target position of 0 cm
22:10-04:00	Low-energy TOF measurement at target position of 0 cm

December 3, 2001

08:57-14:17	Low-energy TOF measurement at target position of +20 cm
14:43-16:25	High-energy TOF measurement at target position of +20 cm
16:35-18:02	High-energy TOF measurement at target position of +40 cm
18:21-18:51	High-energy TOF background measurement at target position of +40 cm with detectors 8" out of neutron beam
19:11-02:00	Low-energy TOF measurement at target position of +40 cm

Shipped activation foils to TA-48

December 4, 2001

Removed target from beamline and positioned the target near the wall of the Blue Room, with shielding material to minimize the dose rate near the target.

3.2 Target 4 Irradiations

The foils packets 1 and 14 were placed in the 30L beamline in Bldg 1265 (ICEhouse) about 20 meters from Target 4. A laser was used to ensure alignment of the foils with the neutron beam. The beamline shutter was opened at 9:22 AM on 12/5/01 and the foil irradiation was begun. Monitoring of the beam current was done by the counts in the fission detector, as well as in a computer file of the beam current and fission detector counts. After three days of irradiation, the beam shutter was closed at 11:11 AM on 12/8/01, and the foils were removed and taken the to the staging area for counting. The total neutron exposure is estimated to have been about 4.3×10^{11} n/cm^2.

4. Preliminary Results

4.1 Beam Monitoring

The proton beam was provided by the LANSCE accelerator. The proton beam exited the beamline vacuum through a thin stainless steel window, traveled about 2 meters through air, and then was incident on the target. A primary requirement for the measurement of proton interactions is the determination of the parameters of the incident beam. These parameters include the total integrated beam striking the target assembly in each irradiation, the position of the beam on the target, and the beam intensity profile. The beam monitor system is shown schematically in Figure 2.

To ensure that the target-beam interaction can be accurately modeled, it is necessary to carefully monitor the proton beam position. To accomplish this, a system was implemented to image the proton beam spot on the front face of the target. It is shown in Figure 2 and consisted of a Cr-doped aluminum oxide phosphor indexed and accurately mounted on the target. A thin aluminized Mylar pellicle reflected the light from this phosphor into a lens system that relayed the image to a mirror and then into a shielded camera system consisting of a gated image intensifier and a CCD digital video camera. This system permitted both real-time observation of the beam size and position and also recording of the beam intensity profiles during the course of the irradiation. The image was relayed to the accelerator control room, which permitted the operators to quickly correct any diffuse or dislocated beam spots. Any dislocation of the beam was corrected within 5 minutes of the beginning of irradiation. In all cases the beam spot was maintained within 0.2 cm of the target center.

The incident beam current was monitored in the LANSCE Central Control Room using a standard LANSCE current monitor [9] located in the proton beamline about three meters upstream from the target. A digital reading from this monitor was recorded at 10-second intervals over the course of each irradiation, and the file of current values so generated was used to document the time-dependence of the current and, from its integral, to determine the total number of protons incident on the sample for a given irradiation. The systematic uncertainty in the calibration of this beam monitor is estimated to be about 3%. The monitor reads out with a precision of 1 nanoamp. The nominal current used in this work was about 30 nanoamps, so this adds a second uncertainty of about 3% for an overall uncertainty of about 4.5%.

A second method employing an aluminum activation foil (see Figure 2) was also used to determine the integrated proton fluence on the target assembly for each irradiation. The method employed a stack of three aluminum foils, each nominally 0.32 mm in thickness. The exact thickness of each foil was determined by weighing the foil and carefully measuring its dimensions (nominally 10 cm × 10 cm). Thickness measurements with a micrometer were also used to test the uniformity. Variations over the foil were found to be negligible. The proton beam fluence was then determined by counting the ^{24}Na activation products using a Germanium gamma-ray detector. Only the middle foil in each stack was counted, the presence of the upstream and downstream foils was to ensure

that the center foil was in equilibrium with any recoiling reaction products. The cross section for production of ^{24}Na by 800-Mev protons has been studied previously and has an uncertainty of less than 2% [10]. The half-life for ^{24}Na is 14.9590 hours and the 1.368-Mev gamma ray is produced in 99.9936% of the decays. A calibrated ^{60}Co source was counted simultaneously with the aluminum foil. In this way the activity of the ^{24}Na could be determined by direct comparison of the counting rate with the ^{60}Co source, requiring only a small correction for the difference in energies between the 1.332-Mev gamma ray from ^{60}Co and the 1.368-Mev gamma ray from ^{24}Na. The ^{60}Co source was NIST-traceable with quoted uncertainties of 2% (at the 99% confidence level). The measured activity was corrected for decay after irradiation. A small additional correction for decay of the ^{24}Na during the irradiation (2 to 4 hours) has been applied. Overall uncertainty in the proton beam determination by this method is less than 2%.

For the irradiation of the foil packet, which was to receive a much larger total proton fluence, a second aluminum foil was kept in the beam during the course of the second foil packet irradiation and the setup and data runs for the TOF data. Since the duration of these irradiations were considerably longer than the half-life of ^{24}Na and occurred in a somewhat random sequence, the ^{22}Na activity was counted to determine the total proton fluence. The half-life for ^{22}Na decay is 2.602 years and the 1.275-Mev gamma ray is produced in 99.98% of the decays. The same ^{60}Co source was used in the same manner as for the ^{24}Na activity. Cross sections for production of ^{22}Na were also determined in Ref. 10.

As indicated in Figure 2, a third device was also used to monitor the proton beam current. This was a Bergoz Model ICT-122-070-20:1 integrating current transformer (ICT). The transformer was mounted between the beamline vacuum exit window and the pellicle used in the beam imaging system. The signal was processed by a charge sensitive preamplifier, linear main amplifier, and analog-to-digital converter (ADC). This device measured the charge in each micropulse of the beam and was used for real-time monitoring of the proton beam at the control station for the TOF experiments. Additionally the ADC outputs were stored in a histogram for each irradiation. The centroid of this histogram provided a measure of the average charge per beam pulse. Multiplication by the total number of beam pulses gave the integrated beam charge. This system was calibrated by recording the ADC output for the injection of a known charge into a wire loop through the ICT. Overall uncertainty of this technique was estimated to be 2%, determined mainly by the uncertainty of the injected calibration charge.

Table 8 summarizes the results for the determination of the total number of protons incident on the sample for each of the various irradiations. The values from the three methods were consistent within the estimated uncertainties. The values used to normalize the irradiations were taken to be the weighted average of the values from the three methods and have an uncertainty of less than 2%. Note that for the TOF measurements, only the facility current monitor and the ICT were used to determine total proton fluence.

Table 8. Determinations of Total Proton Fluence

Run	Facility Monitor	Uncertainty (4.5%)	Integrating Current Transformer	Uncertainty (2%)	Aluminum Activation	Uncertainty (2%)	Weighted Average	Uncertainty Absolute	Uncertainty (%)
First foil irradiation	1.40×10^{15}	6.3×10^{13}	1.41×10^{15}	2.8×10^{13}	1.40×10^{15}	2.8×10^{13}	1.40×10^{15}	1.9×10^{13}	1.3
Second foil irradiation	2.27×10^{15}	1.0×10^{14}	2.31×10^{15}	4.6×10^{13}	2.29×10^{15}	4.6×10^{13}	2.30×10^{15}	3.1×10^{13}	1.3
High-energy neutron TOF, target position 0 cm	6.53×10^{14}	2.9×10^{13}	6.26×10^{14}	1.3×10^{13}	—	—	6.30×10^{14}	1.2×10^{13}	1.8
Low-energy neutron TOF, target position 0 cm	3.54×10^{15}	1.6×10^{14}	3.28×10^{15}	6.6×10^{13}	—	—	3.32×10^{15}	6.1×10^{13}	1.8
High-energy neutron TOF, target position +20 cm	6.53×10^{14}	2.9×10^{13}	6.51×10^{14}	1.3×10^{13}	—	—	6.51×10^{14}	1.2×10^{13}	1.8
Low-energy neutron TOF, target position +20 cm	2.88×10^{15}	1.3×10^{14}	2.99×10^{15}	6.0×10^{13}	—	—	2.97×10^{15}	5.4×10^{13}	1.8
High-energy neutron TOF, target position +40 cm	6.82×10^{14}	3.1×10^{13}	6.81×10^{14}	1.4×10^{13}	—	—	6.81×10^{14}	1.2×10^{13}	1.8
Low-energy neutron TOF, target position +40 cm	3.79×10^{15}	1.7×10^{14}	3.72×10^{15}	7.4×10^{13}	—	—	3.73×10^{15}	6.8×10^{13}	1.8
Long foil irradiation	—	—	1.55×10^{16}	6.2×10^{14}	1.57×10^{16}	3.1×10^{14}	1.57×10^{16}	2.8×10^{14}	1.8

4.2 Initial Foil Counting

The initial foil counting was performed in the LANSCE staging area in three phases. The first phase was the counting of foil packet #5 after the initial irradiation on Saturday, Dec. 1. This was performed to confirm the efficacy of the experiment, including the length of the irradiation, beam current, foil sizes, activity of the foils at extraction, etc. This phase was performed successfully and demonstrated that the foils would have sufficient activity to gather the desired data. In addition, it was learned that there appeared to be little benefit in using Cd-covered Au foils. The covered and uncovered foils showed very little difference in activity. In addition, because of the substantial mass and large cross section of cadmium, the cadmium foil contributed significantly to the overall radioactivity of the foil packet. On this basis, it was decided to remove the cadmium-wrapped gold foils from all but two (1 and 13) of the foil packets. Packet 13 contained only Au and Cd-covered Au and was placed on the table beneath the LBE target to measure any thermal flux from the general room.

The next phase of counting was performed after the irradiation on Sunday, Dec. 2. Multiple foils were irradiated and withdrawn at this point. Given the large number of foils to be counted, it was decided to count first the Bi and Tb foils from locations along the length of the target. This was done to ensure several short-lived isotopes in these materials were sampled from several locations. The next day these foils were packaged and sent to TA-48 for counting.

After completion of the TOF phase of the experiment, two foil packets (3 and 12) that had been left on the target for the duration of the irradiations were withdrawn. Counting then began on all the materials in these packets at the staging area. Although the foils were not withdrawn until more than 9 hours after beam shut-off, the long irradiation time guaranteed sufficient activity was available and many different isotopes were identified for each material.

The initial work on configuring the software and libraries for *PCGAP* has been completed, although several additional tasks remain to be completed before the final data analysis of the various spectra can be performed. A preliminary analysis has been performed using the Bi foils that were taken from the target and counted on Sunday, Dec. 2. The activities of the various Bi isotopes as a function of position along the target are shown in Figure 12. It can be seen that there is a consistent trend in the results. The peak activity, and hence flux, occurs around 10 cm, which is consistent with the Monte Carlo calculations. Figure 13 shows the activities for several Bi isotopes normalized to 1 at 10 cm. These results indicate that the larger mass isotopes (205, 206, 207) drop off more quickly than the lower mass isotopes (199, 200, 201) as a function of axial position. This can be attributed to a hardening of the neutron spectra further down the target. The higher-energy neutrons are more strongly forward scattered. One possible anomaly in the results is the Bi-199 activity at 30 cm. The activity seem to be higher than can be attributed to a harder spectrum above 100 MeV (the threshold for the n,11n reaction).
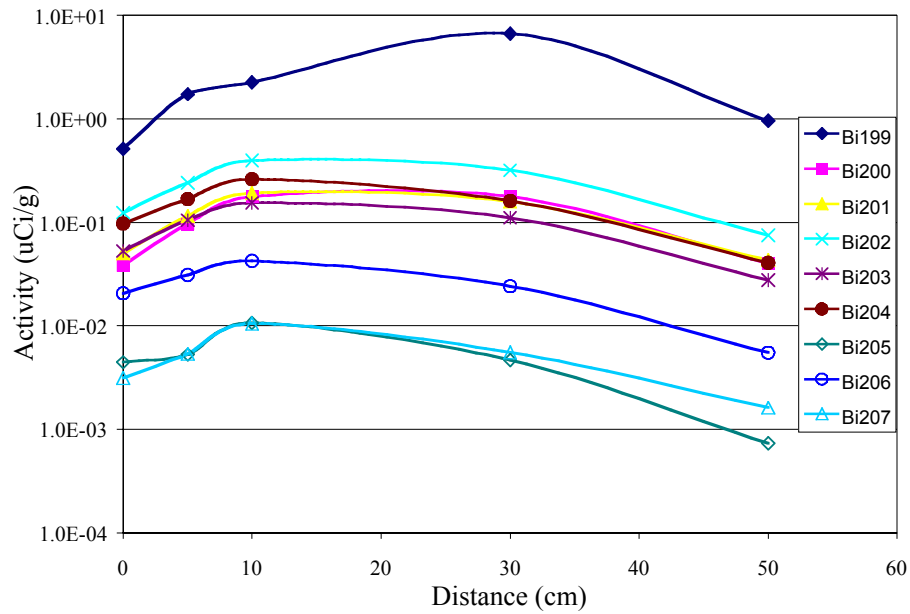
Figure 12. The activity of bismuth isotopes as a function of distance along the target.
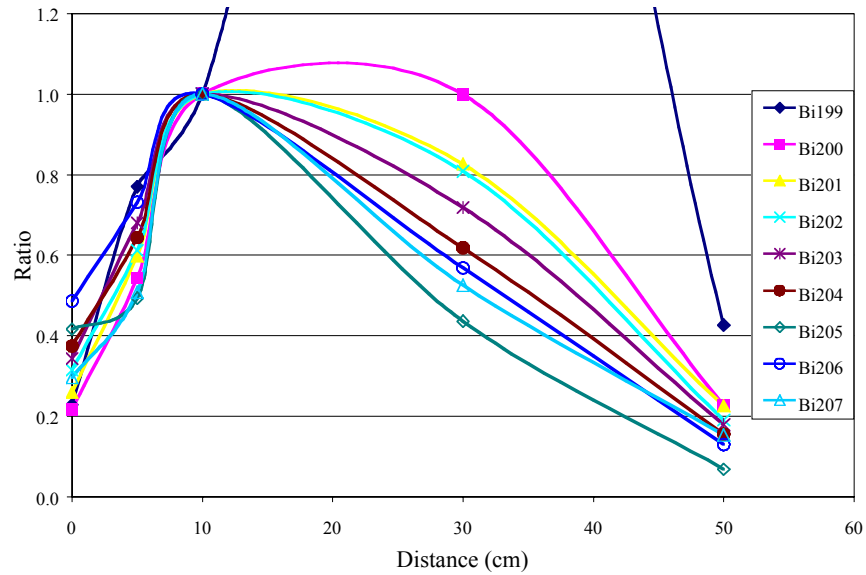

Figure 13. The ratio of activities for bismuth isotopes normalized to 1 at 10 cm.

4.3 Nuclide Identification

Most of the irradiated foils present a very complex set of lines when presented to one of the High-Purity Germanium detectors (HPGe). Prior to entrusting the analysis of this large amount of data to prepackaged software, the initial analysis focused on a review of the spectra and individual identification of peaks and peak energy. The experience acquired in this way is invaluable in completing the analysis of the present experiment and is used to generate the necessary gamma spectral data library. This library is used by the software to perform automated peak fitting and identification.

In a first stage, spectra obtained from a typical bismuth foil were searched for lines expected from several possible reactions. The isotopes identified in the Bi foils are listed in Table 9.

Table 9. Some Nuclides Identified in Bismuth Activation Foils

Gamma Energy (keV)	Nuclide	Branching Ratio (%)	Half-life (hrs)
881	Bi-206	66.00	150
842	Bi-199	11.00	0.45
825	Bi-203	14.60	11.8
820	Bi-203	29.60	11.8
803	Bi-206	98.90	150
787	Pb-202m	50.00	3.53
720	Pb-199	6.50	1.5
703	Bi-205	31.10	367
670	Bi-204	11.40	11.2
657	Pb-202m	32.40	3.53
636	Tl-198	10.10	5.3
629	Bi-201	24.00	1.8
620	Ac-228	Background (see note 2)	
609	Bi-214	Background (see note 2)	
587	Tl-198	0.20	5.3
578	Tl-197	4.40	2.84
537	Bi-206	30.50	150
516	Bi-206	40.70	150
511	Annihilation		
497	Bi-206	15.00	150
490.5	Pb-202m	9.10	3.53
462	Bi-200	98.00	0.6
425	Bi-199	22.00	0.45
422	Pb-202m	86.00	3.53
420	Bi-200	91.00	0.6
412	Tl-198m	57.00	1.87
412	Tl-198	82.00	5.3
412	Au-198	95.58	65
375	Bi-204	82.00	11.2
367	Pb-199	44.00	1.5

Gamma Energy (keV)	Nuclide	Branching Ratio (%)	Half-life (hrs)
353	Pb-199	9.50	1.5
338	Ac-228	Background (see note 2)	
331	Pb-201	79.00	9.33

Notes:
1. It is assumed that Pb-202m is produced directly, although it can result from the decay of Bi-202 with $T_{1/2}$ = 1.72 Hr.
2. The second spectrum was taken with an unshielded detector for a much longer period of time. Hence, some of the background lines show up more than in the earlier spectrum.

Figures 14 to 16 show details of three different energy ranges. The same foil was counted shortly after the irradiation and again about 20 hours later. The spectra being compared were taken with two different detectors and counted for different durations. The data were normalized using two peaks of ^{206}Bi, at 803 and 881 keV, as shown in Figure 14.
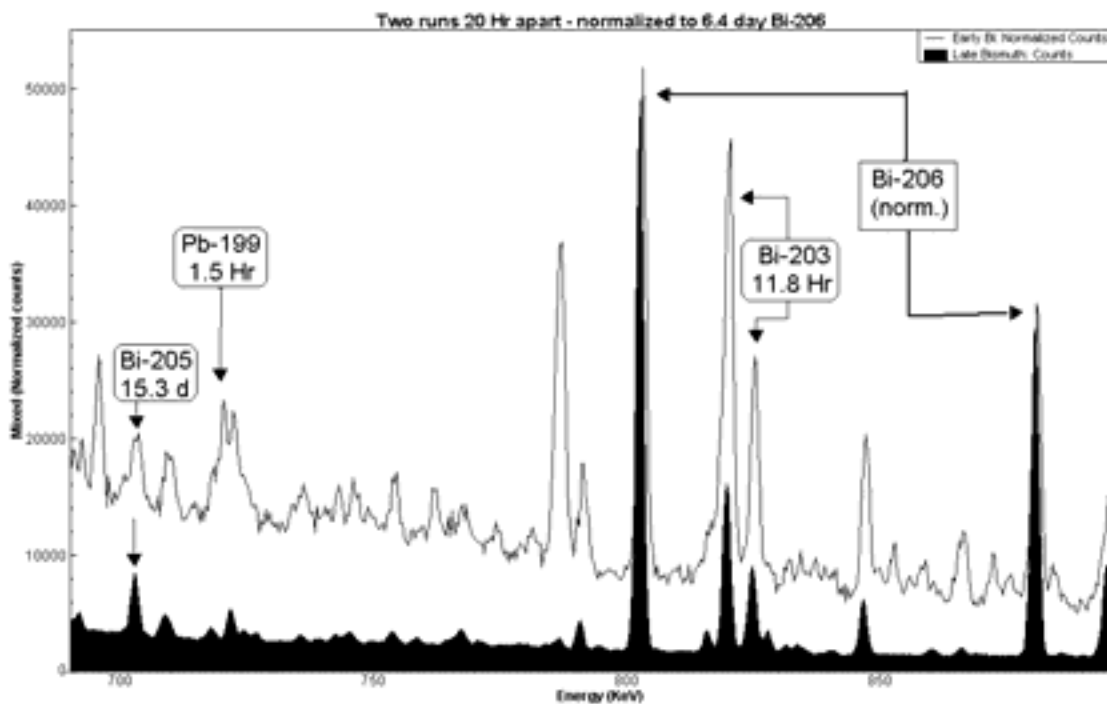

Figure 14. The 700 to 900 keV region of a bismuth foil measured twice at about a 20-hour interval. The cross-normalization was obtained by matching the two peaks of long-lived ^{206}Bi at 803 and 881 KeV.
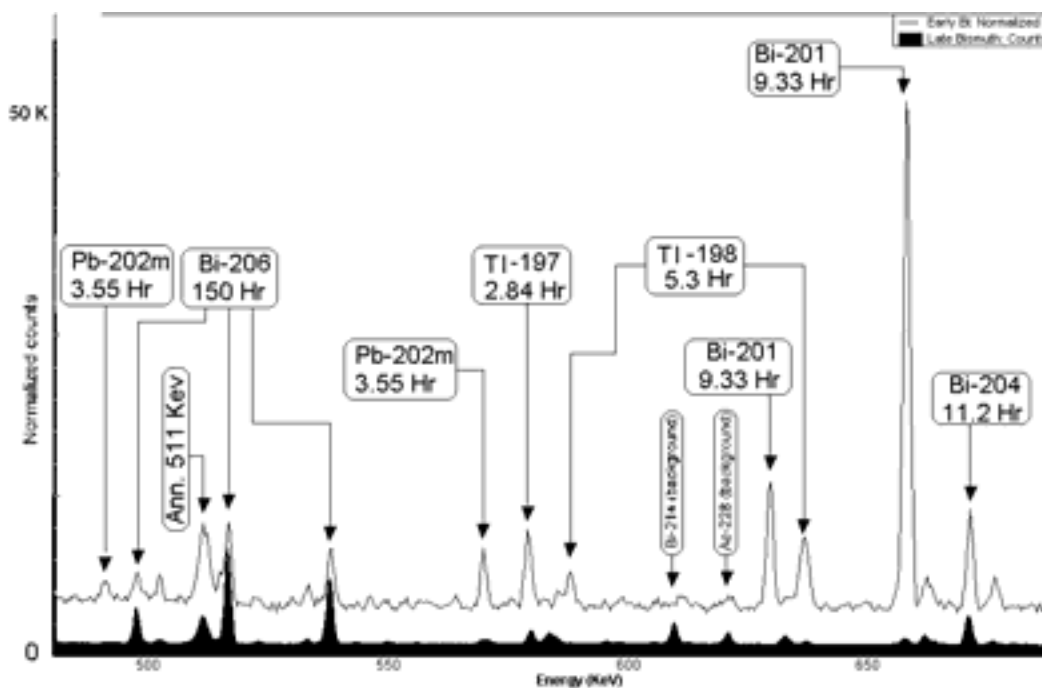
Figure 15. Continuation of the spectra shown in Figure 12. Region from 480 keV to 680 keV.
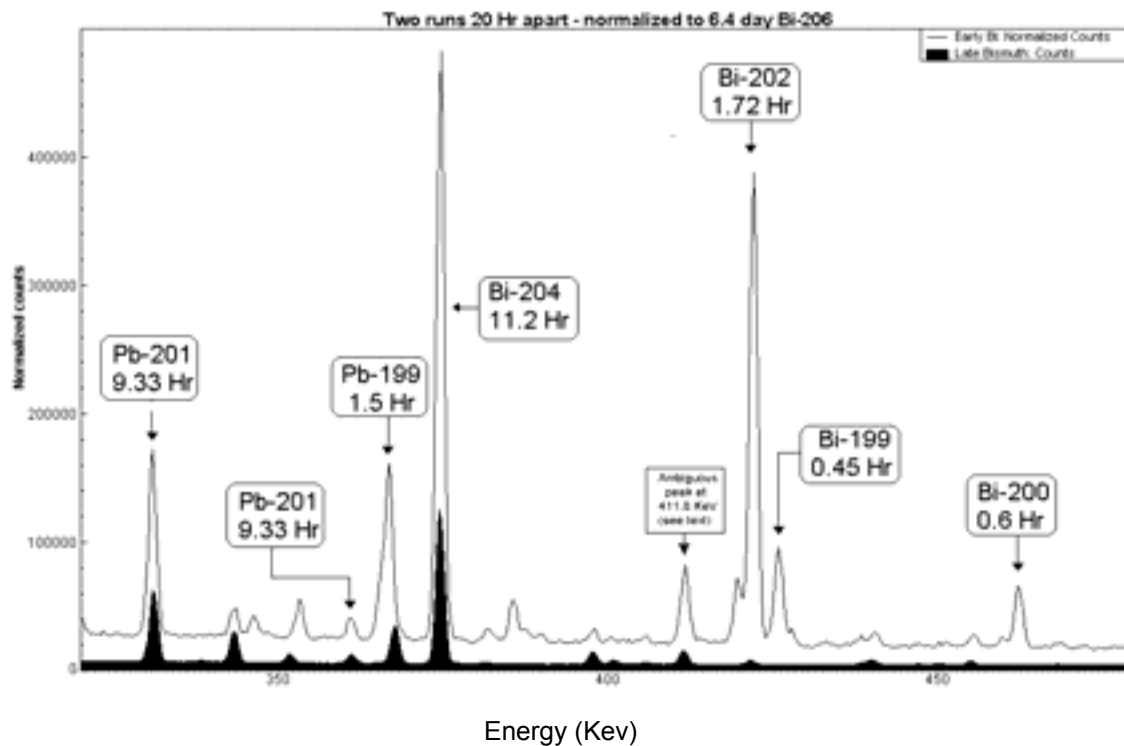

Energy (Kev)

Figure 16. Continuation of the spectra shown in Figure 13. Region from 320 keV to 480 keV.

Most peaks can be attributed to nuclides produced by neutrons interacting with the ^{209}Bi nuclei in the foil. Peaks are labeled with the corresponding nuclide and its accepted half-life. The disappearance or decrease in intensity of the peaks belonging to the short-lived activities (a few hours) reinforces confidence in the identification obtained from multiple gamma peaks. In the future, quantitative half-life determination (or consistency) can be performed for many of the samples.

For bismuth, there are two potentially ambiguous cases:

1. The 411.8-keV peak (shown in Figure 16) illustrates the ambiguities due to the existence of three plausible gamma lines: ^{198}Tl ($T_{1/2}$ = 5.3 Hr), the isomer ^{198m}Tl ($T_{1/2}$ = 1.87 Hr), and ^{198}Au ($T_{1/2}$ = 2.7 days), all three corresponding to the same transition from the first excited level of ^{198}Hg. Such an ambiguity can be lifted if one has detailed information about the half-lives and/or by using the abundance deducted from measurements of other lines of the same nuclide. The former requires several strategically timed measurements, and the latter relies on the accurate knowledge of the energy-dependence of the detector's efficiency.

2. ^{200}Bi ($T_{1/2}$ = 0.6 Hr) and ^{199}Bi ($T_{1/2}$ = 0.45 Hr) have unresolved lines around 420 keV. Here again, having several measurements at short intervals may help resolve the source of the gamma lines.

In bismuth, the following reactions have been observed via several of the most abundant gamma lines of the final nuclide.

$$^{209}\text{Bi (n, } x \text{ n) } ^{210 - x}\text{Bi} \qquad \text{for } x = 4 \text{ to } 10$$

with positive identification of ^{200}Bi (3 lines), ^{201}Bi (5 lines), ^{202}Bi (6 lines), ^{203}Bi (4 lines), ^{204}Bi (7 lines), ^{205}Bi (4 lines), and ^{206}Bi (6 lines).

Four lines of ^{198}Tl ($T_{1/2}$ = 1.87 Hr) have been found, corresponding to

$$^{209}\text{Bi (n, 2p 10n) } ^{198}\text{Tl}.$$
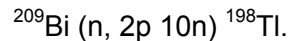
^{209}Bi (n,p xn) $^{209-x}$Pb for x = 8 and 10 was also observed from the signature of ^{199}Pb (3 lines) and ^{201}Pb (3 lines).

While this preliminary analysis focused on the identification of as many lines as possible, our ultimate goal is the validation of Monte Carlo predictions of the neutron spectrum produced in the Pb-Bi target. For this, the accurate measurement for each reaction threshold of the activity of one or two well-understood gamma lines is all one needs to determine the validity of the code used. Half-life information and the presence of other expected lines only provide confirmation of the origin of those selected lines one retains to extract the quantitative information.

Our analysis shows that in the case of bismuth, there are enough reliable gamma rays to carry out our intended purpose.

4.4 Time-of-Flight Measurements

Two data acquisition sequences were performed at each of the three target positions. These target positions were with the face of the target at 0 cm, 20 cm (upstream), and 40 cm with respect to the intersection of the proton beam axis and flight path axes. The first data acquisition sequence used the plastic detectors to obtain data in the high-neutron-energy region (~0.5 to 800 MeV). This required about 1.5 hours of beam (~20 nanoamps) on target at each target position and used 20 microsecond spacing for the beam pulses. The second sequence used the Li-loaded glass detectors to obtain data in the lower-energy region (~0.01 to 1 MeV). About 8 hours of beam time (~25 nanoamps) were required for each target position with a beam-pulse spacing of 40 microseconds.

Examples of TOF spectra for the first target position (target face at 0 cm) are shown in Figures 17 and 18. The data shown here are for detector distances of 51.15 and 29.85 m at angles of 7.5° and 30°, respectively. The corresponding fields-of-view at the center of the target assemblies are 11.07 and 11.71 cm in diameter.
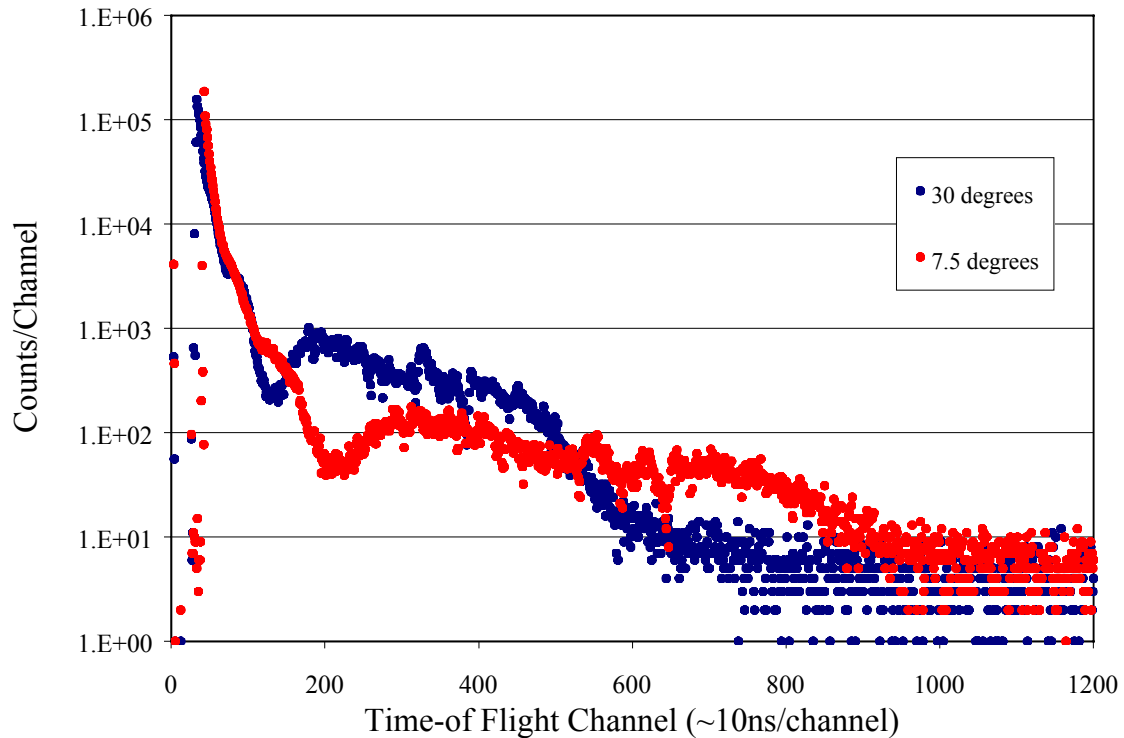

Figure 17. Time-of-flight spectra measured with the Li-loaded glass (low-energy) detectors for the target position at 0 cm. The data are for 7.5° and 30°.
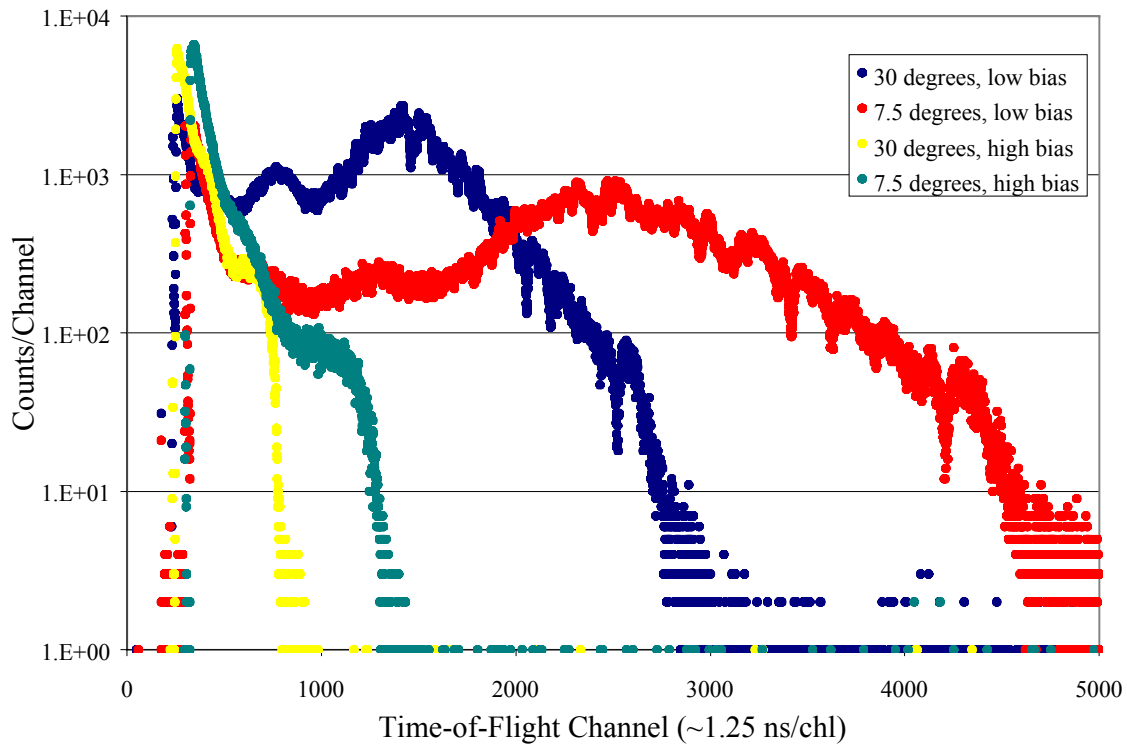
Figure 18. Time-of-flight spectra measured with the plastic (high-energy) detectors for the target position at 0 cm. The data for 7.5° and 30° are shown for each of two pulse height thresholds on the detectors.

The raw data shown in the figures consist of count rate as a function of time-of-flight. Subsequent analysis of these data will be needed to correct for experimental characteristics such as the detector efficiencies and system dead times to produce absolute neutron intensities as a function of neutron energy, normalized to unit incident proton. Energy bins will be selected to make the best use of the available counting statistics to optimize both energy resolution and intensity uncertainty. The separate data sets for the various detectors and bias settings will be merged to form one neutron energy spectrum for each target position. A preliminary analysis of the raw data has been performed, and the TOF neutron-energy spectra are shown in Figures 19 through 21.
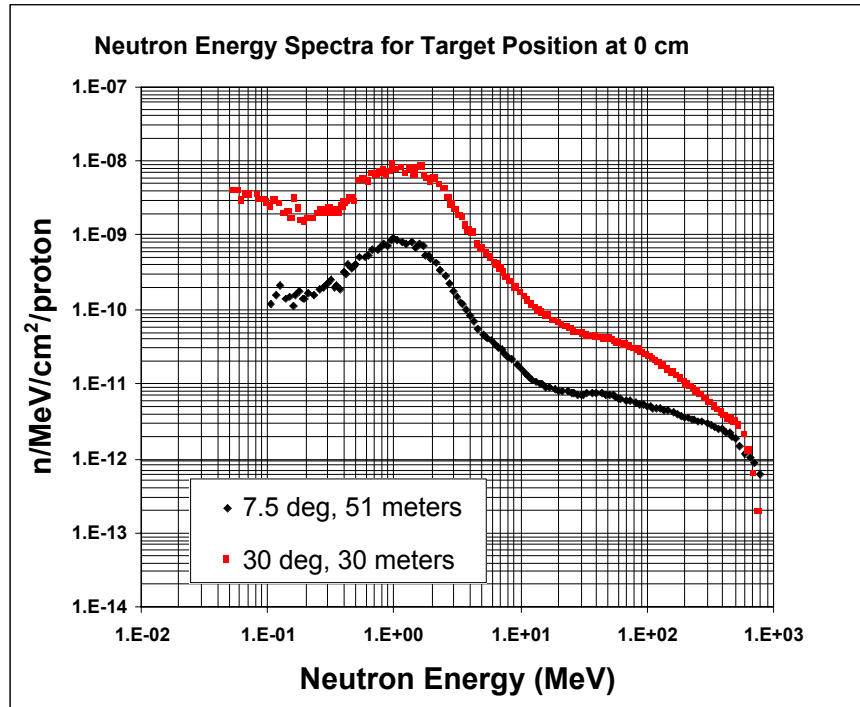
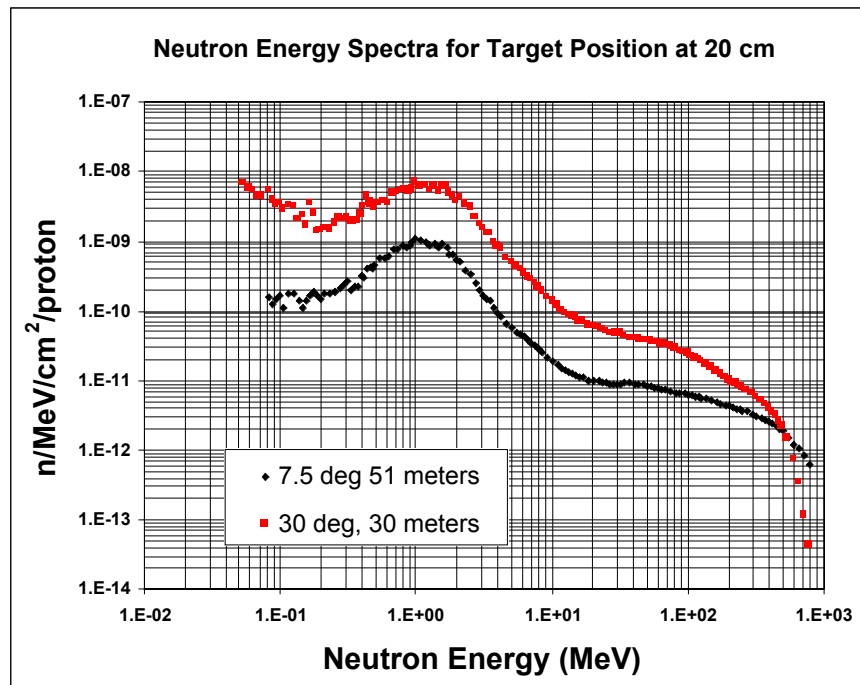**Figure 19. Time-of-flight neutron-energy spectra for target position at 0 cm.**

Figure 20. Time-of-flight neutron-energy spectra for target position at 20 cm.
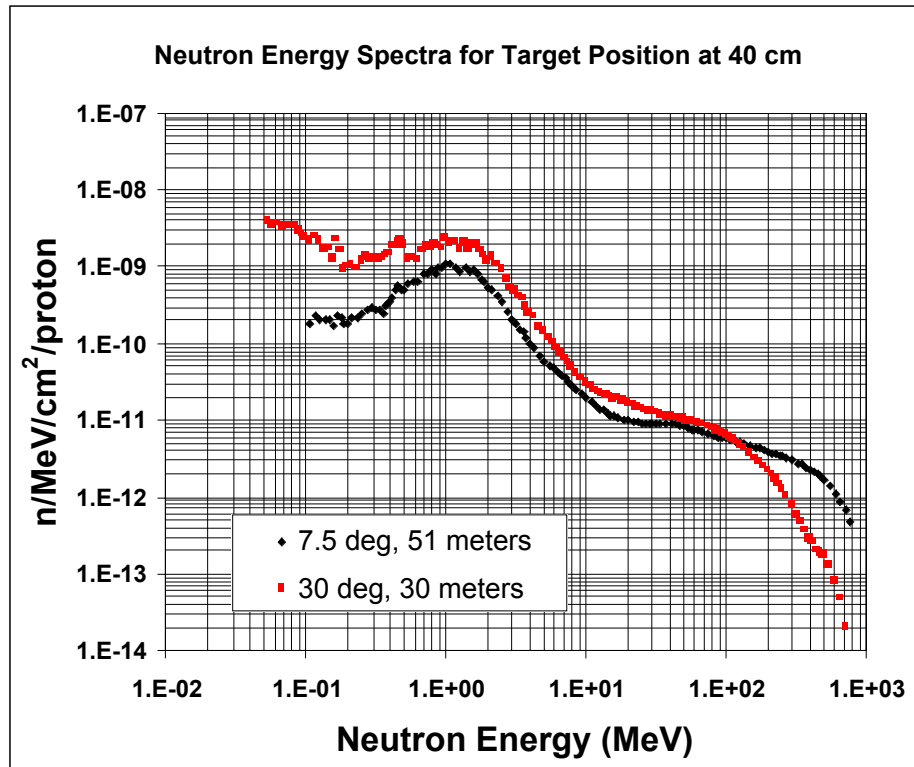
Figure 21. Time-of-flight neutron-energy spectra for target position at 40 cm.

4.5 TA-48 Counting

After an initial counting in the staging area, a number of the foils were sent to TA-48 to be counted by the C-INC group. The foils shipped over were packet 5, which was irradiated on Saturday, Dec. 1 for about 2 hours at 26 nA of proton beam. Also shipped over were foil packets 2, 4, 6, 7, 8, 9,10, 11, 12, and 13. It was not possible to perform extensive counting on all these foil packets in the staging area, so focus was made on getting the Bi foil counted from packets along the length of the target. After evaluation of an initial counting of all the foils, several foils were chosen for follow-up counting based on insufficient data in the spectra.

4.6 Target 4 Results

The final phase of counting was performed on the Target 4 foils that were withdrawn on Sunday, Dec 8. These foils had been exposed to a low neutron flux for approximately three days. It was discovered that for many foils, the levels of activity were much too low to be useful, so the counting was focused on the high-Z elements such as Lu, Tb, Bi, In, and Au where sufficient activity existed to gather good data.

Initial results from the counting on the Target 4 foils revealed that the activities were very low. This was expected, as the neutron fluxes in the foil location are ~ 1×10^6 n/cm^2/s.

From the initial results, only the higher-Z foils produced noticeable peaks that could be used for analysis. But the Bi, Lu, Tb, In, and Au all gave some initial results, including several of the higher n,nx reactions in the Bi.

5. Summary

Initial experiments were conducted at the Target 2 facility (commonly called the Blue Room) at LANSCE to support the Advanced Accelerator Applications Program. The experiments consisted of irradiating a solid lead-bismuth target (diameter=20 cm, length=50 cm) with the 800-Mev proton beam and measuring the neutron emission from the target by two different methods—activation foils and TOF measurements.

The irradiations and TOF measurements were conducted without incident and with minimal personnel exposure. Preliminary results indicate that both techniques for measuring the neutron leakage provide useful and complementary information. The activation foils provide significant quantities of integral reaction data that can be used for spectral unfolding, with errors representative of the uncertainties in the nuclear data. The TOF measurements provide very detailed information regarding the neutron spectra in a small solid angle (i.e., double differential data).

The goals of the initial target irradiation experiment were to:

1. provide initial experimental data for planning future irradiation campaigns,

2. provide experimental data of benchmark quality to be used for validation of MCNPX,

3. provide experimenters with practical experience for conducting these types of measurements and data analysis activities, and

4. further develop methods and improve techniques for spectral unfolding using integral reaction data from activation foils.

Although it will be some time before the large amounts of data can be properly reviewed and analyzed, it is apparent that the goals and intent of the initial irradiation experiment have been accomplished.

The initial irradiations provide data that are invaluable to planning future irradiation campaigns and analysis activities. The data will help better define the necessary irradiation times, foil packet locations, and other relevant parameters for irradiation. It is also valuable in providing detailed gamma spectra for review and identification of product isotopes. This will greatly decrease the analysis times in the future as peaks of interest will already be identified.

Meticulous records of the experimental geometry and analysis of the data have been recorded. The records and results are of sufficient quality to include in a benchmark. The development of a benchmark report will begin in earnest.

All researchers involved gained valuable experience in the conduct of activities at the LANSCE Blue Room and the involvement and coordination with the different groups at the LANSCE facility and at LANL. In addition, the experience in handling and counting

the activation foils at LANSCE will greatly increase the efficiency and conduct of counting activities for future irradiation campaigns.

Finally, the identification of peaks from target irradiations will serve to assist in the development and improvement of techniques for spectral unfolding. The identification of gamma peaks, and isotopes of interest from these initial irradiations, will allow a more thorough review of the production reactions and cross-section data. This review will allow a systematic approach to the improvement of the spectral unfolding process, through the identification of deficiencies in dosimetry cross-section data, the unfolding process, and the identification of reaction data that provide similar results, i.e., the reactions can be used to check for consistency in counting results and flux determination, and the number of foils can be reduced in future irradiations—thereby saving time and effort by eliminating redundant information.

Future irradiations will include additional beamlines and full complements of activation foil packets. Because of the additional data requirements, experience gained from this initial irradiation sequence is invaluable in helping plan and organize future irradiations. Based on the results from this initial irradiation, planning efforts for the next irradiation cycle can now begin.

6. References

1. M.M. Meier, C.A. Goulding, G.L. Morgan, and J.L. Ullmann, "Neutron Yields from Stopping- and Near-Stopping-Length Targets for 256-MeV Protons," *Nucl. Sci. Eng.* **104**, 339 (1990).

2. M.M. Meier, D.A. Clark, C.A. Goulding, J.B. McClelland, G.L. Morgan, C.E. Moss, and W.B. Amian, "Differential Neutron Production Cross-Sections and Neutron Yields from Stopping-Length Targets for 113-MeV Protons," *Nucl. Sci. Eng.* **102**, 310 (1989).

3. M.M. Meier, W.B. Amian, C.A. Goulding, G.L. Morgan, and C.E. Moss, "Neutron Yields from Stopping-Length Targets for 256-MeV Protons," *Nucl. Sci. Eng.* **110**, 299 (1992).

4. M.M. Meier, W.B. Amian, C.A. Goulding, G.L. Morgan, and C.E. Moss, "Differential Neutron Production Cross Sections for 256-MeV Protons," *Nucl. Sci. Eng.* **110**, 289 (1992).

5. W.B. Amian, R.C. Byrd, C.A. Goulding, M.M. Meier, G.L. Morgan, C.E. Moss, and D.A. Clark, "Differential Neutron Production Cross Sections for 800-MeV Protons," *Nucl. Sci. Eng.* **112**, 78 (1992).

6. W.B. Amian, M.M. Meier, R.C. Byrd, C.A. Goulding, G.L. Morgan, and C.E. Moss, "Efficiency Calibration of a Cylindrical BC418 Neutron Detector at Neutron Energies Between 135 and 800 MeV," *Nucl. Instrum. Methods* **A313**, 452 (1992).

7. W.B. Amian, R.C. Byrd, D.A. Clark, C.A. Goulding, M.M. Meier, G.L. Morgan, and C.E. Moss, "Differential Neutron Production Cross Sections for 597-MeV Protons," *Nucl. Sci. Eng.* **115**, 1 (1993).

8. G. Morgan, G. Butler, M. Cappiello, S. Carius, L. Daemen, B. DeVolder, J. Freshut, C. Goulding, R. Grace, R. Green, P. Lisowski, P. Littleton, J. King, N. King, R. Prail, T. Stratton, S. Turner, J. Ullmann, F. Venneri, and M. Yates, "LANL Sunnyside Experiment: Study of Neutron Production in Accelerator-Driven Targets", International Conference on Accelerator-Driven Transmutation Technologies and Applications, *AIP Conference Proceedings* **346**, 682 (1994).

9. F.R. Gallegos, *Development of a Low Intensity Current Monitor System*, Los Alamos National Laboratory report LA-UR-91-3400 (1991).

10. G.L. Morgan et al., "Total Cross Sections for Production of ^{22}Na and ^{24}Na in Proton-Induced Reactions on ^{27}Al from 0.4 to 22 GeV," to be published in *Nucl. Sci. Eng.*

7. Acknowledgments

This work has benefited from the use of the Los Alamos Neutron Science Center at Los Alamos National Laboratory. This facility is funded by the US Department of Energy under Contract W-7405-ENG-36.

APPENDIX A

Analysis from the lead-bismuth target conducted after pouring from a small sample of the target material

Luvak Inc.
722 Main Street
P.O. Box 597
Boylston, MA 01505
508-869-6401

Analytical report no.
0-24975
Page 1 of 1

Requested by:
Los Alamos National Laboratory
Los Alamos Neutron Science Center
Los Alamos, New Mexico 87545

Attention:
Valentina Tcharnotskaia
LANSCE-3, M/S H855
Amended Report

Invoice number: 39718
Customers Purchase Order no.: Credit Card

Date received: 05/24/01
Invoice date: 06/01/01
Report date: 06/01/01
Amended date: 06/05/01

Description: One Lead-Bismuth Eutectic sample was analyzed as listed below.

Results:

Sample Identification:	SM 200127698
	%
Mercury	<.00005
Thallium	<.001
Arsenic	.010
Boron	.012
Barium	.001
Bismuth	55.8
Cadmium	.001
Copper	.025
Iron	.008
Gallium	.003
Molybdenum	.003
Sodium	.001
Niobium	.016
Phosphorus	.020
Lead	43.7
Antimony	.029
Silicon	.006
Tin	.032
Strontium	.001
Tantalum	.006
Titanium	.006
Vanadium	.009
Zinc	.001
Zirconium	.019

LUVAK INC.

By _____